Electron Drift Velocities in Liquefied Argon and Krypton at Low Electric Field Strengths

HAROLD SCHNYDERS,* STUART A. RICE,† AND LOTHAR MEYER
Department of Chemistry and Institute for the Study of Metals, University of Chicago, Chicago, Illinois
(Received 25 April 1966)

In this paper we report measurements of the drift velocity of electrons in liquid Ar and Kr as a function of temperature, pressure, and electric field strength. The experimental findings are as follows: (a) At low temperatures (<115°K) in liquid Ar, the mobility of the electron (~400 $cm^2 V^{-1} sec^{-1}$) decreases with increasing temperature and increases with increasing pressure. In this region the electron drift velocity is linear in the electric field strength (from −100 to −200 V/cm). (b) At high temperatures (>115°K) in liquid Ar and at all temperatures in liquid Kr the electron drift velocity (4–20×10^4 cm/sec) at electric field strengths from −50 to −150 V/cm *increases* with increasing temperature. There may be a maximum in the electron drift velocity-temperature profile of liquid Kr. In this region the drift velocity is *not* linear in the electric field strength. It is demonstrated that an elementary scattering theory (with several variants for the scattering cross section) provides a reasonable *zeroth*-order description of the electron mobility in liquid Ar in the low-field, low-temperature (<115°K) region. The theory incorporates the effects of coherence in the electron scattering from nearby atoms into the cross section of a modified Boltzmann equation. The magnitude of the mobility and the pressure and temperature dependence (85–115°K in liquid Ar) of the mobility are all reproduced to better than a factor of 2. It is found that the electron velocity distribution is *not* thermal and that the mean electron energy may be as large as 0.5 eV, even when the electric-field strength is as low as 100 V/cm. By numerical calculation based on the elementary scattering theory, we find the onset of nonlinearity in the electric-field dependence of the electron drift velocity at $E \approx 1$ V cm^{-1} in disagreement with the experimental findings described in (a). The anomalous rise of the drift velocity per unit field in liquid Ar above 115°K, and at all temperatures in liquid Kr, intuitively suggests that there may be a Ramsauer minimum in the effective electron-atom scattering cross section in the liquid. Within the framework of the elementary theories considered, we have, at present, no explanation for the anomalous temperature dependence of the electron drift velocity in liquefied Ar and Kr.

I. INTRODUCTION

THE nature of the electronic states in dense, irregular systems has been a subject of continuing interest and study since the discovery of the solubility of alkali metals in liquid ammonia one hundred years ago.[1] The study of electron transport in these systems effectively probes and elucidates the strength and nature of the intermolecular interactions. Of course, it is hoped that an understanding of the role of liquid structure in determining the characteristics of electron motion will lead to a general understanding of the electronic states of the system. The first step required in the understanding of electron transport and electron binding in complex liquid systems, such as metal-molten salt mixtures, liquid metals, liquid metallic alloys, liquid ammonia, liquid polar organic semiconductors, and hydrocarbons, is the extensive study of those liquid systems which, in principle, are simplest to understand. The liquid rare gases fit the description of a "simple" fluid for the following reasons:

(1) The species Ar and Kr are monatomic. The absence of vibrational and rotational degrees of freedom insures that inelastic collisions can only be significant at mean electron energies of the same order of magnitude as the first electronic excitation energy in argon or krypton (approximately 10 eV in argon). From the calculated values for the mean electron energy given in Table IV of this paper, it is clear that at the electric field strengths used in our experiments inelastic collisions will play an insignificant role in the over-all scattering process. Thus, the electrons in these simple fluids undergo elastic collisions only. Such collisions are more amenable to theoretical study than are inelastic collisions or a complex combination of the two processes.

(2) The single-atom scattering potential is spherically symmetric.

(3) The interaction between Ar (or Kr) atoms and electrons is relatively weak and of short range.

(4) There are no known stable bound states for an electron with the neutral atomic species Ar and Kr.

(5) The resistivities of these liquids are high (approximately 10^{19} Ω·cm). This permits the use of a sufficiently small concentration of excess electrons (10^3–10^5 cc^{-1} in our experiments) to justify the neglect of electron-electron interaction from theoretical consideration.

There are, of course, other compelling reasons for the study of electron transport in these particular fluids. Although it occurred to us only after the first puzzling experimental data became available, it would naturally be interesting to study the effect of the density of the medium on the Ramsauer-Townsend effect, a property unique to the rare gases.[2] Since the mobility is (roughly) inversely proportional to the elastic-scattering cross

* Present address: Argonne National Laboratory, Argonne, Illinois.

† During 1965–66: N. S. F. Senior Postdoctoral Fellow and Visiting Professor, Université Libre de Bruxelles.

[1] G. Lepoutre and M. J. Sienko, *Metal Ammonia Solutions* (W. A. Benjamin, Inc., New York, 1964).

[2] H. S. Massey and E. H. S. Burhop, *Electronic and Ionic Impact Phenomena* (Oxford University Press, Oxford, England, 1952).

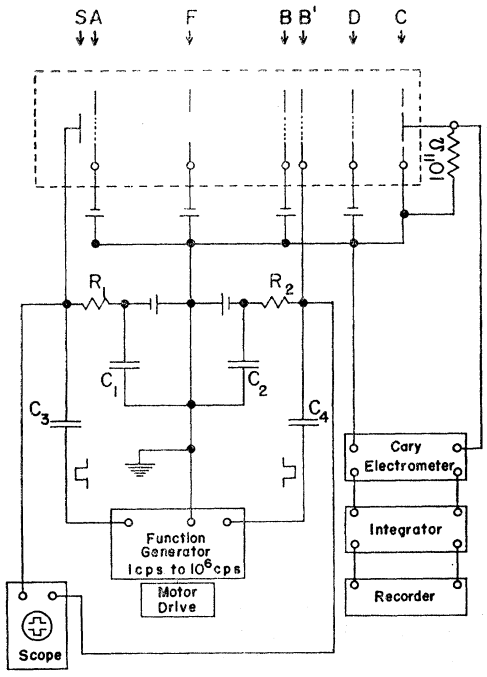

FIG 1. A schematic diagram of the grid system and the external circuits for electrical shutter control and current measurement. The guard ring E helps to maintain a uniform electric field in the main drift space AB. The grounded shell surrounding the collector shields it from the varying field lines generated by the shutter grid B′ which circumvent the D grid. The system enclosed in the dashed line is immersed in the liquid under study.The values of the resistances and capacitances are: $R_1=R_2=1.5$ MΩ, $C_1=C_2=4$ μF, $C_3=C_4=2.02$ μF.

section,[3] the Ramsauer-Townsend effect should be reflected in the electron-drift velocity data, if the single-atom elastic-scattering cross section is not greatly modified in the liquid phase.

Malkin and Schultz,[4] Williams,[5] and Swan[6] have previously measured electron-drift velocities in liquid argon. Their measurements were made with fields in excess of 1 kV/cm, a region in which the electron drift velocity is definitely nonlinear with respect to the electric field strength. Swan has summarized the data on drift velocities in liquid argon, as measured by several experimentalists, in Fig. 2 of his paper.[6] All of the curves in this figure are cut off at electric field strengths of the order of a few kilovolts/cm, and they must be extrapolated to the origin. This leads to a number of different limiting slopes (the mobility) as E, the electric field strength, approaches zero. It is of importance to find the correct slope of the linear region of these curves, for it is precisely in this range of electric field strengths that the field energy of the electron is small compared to its thermal energy, and most available theories are valid only for the description of the zero-field mobility. In this paper we present data for this low-field region.

Excess electrons in a quasifree state have never previously been observed at low-field strengths in the liquefied rare gases. Davis, Rice, and Meyer observed only ions in the liquids argon, krypton, and xenon.[7]

For liquid helium, considerable evidence has accumulated, both experimental[8–11] and theoretical,[12–14] supporting the conclusion that the negative species in this fluid is an electron, albeit a localized electron bound within a void created in the fluid. In this paper we present the first evidence supporting the concept that an electron exists in a quasifree state in the liquefied rare gases (other than He) at low electric field strengths.

II. EXPERIMENTAL DETAILS

The electron-drift velocity, v_d, was determined by a time-of-flight method. The electrical apparatus used in the time-of-flight measurement is shown schematically in Fig. 1. It is similar to the apparatus used by other experimentalists for the study of ion mobilities in gases[15] and in liquids.[8,16] In our first series of measurements, the electron source S was a 400-μCi Po^{210} alpha emitter[17] (the range of the alpha particles in liquid rare gases is of the order of a few tenths of a millimeter). In our last series of measurements, the excess electrons were generated by field emission tips[18,19] mounted according to the description of Henson,[20] who used field emission tips as a positive-ion source for mobility studies in liquid argon and nitrogen. Currents as large as 10^{-6} A can be collected at the first grid surrounding a tip.[21] However, in our experimental arrangement both sources yield approximately the same current (10^{-11} to 10^{-12} A) at the collector C.

The grid system, with which the times of flight of the electrons were measured, is enclosed by the dashed lines

[3] L. S. Frost and A. V. Phelps, Phys. Rev. **136**, 1538 (1964).
[4] M. S. Malkin and H. L. Schultz, Phys. Rev. **83**, 1051 (1951).
[5] R. L. Williams, Can. J. Phys. **35**, 134 (1957).
[6] D. W. Swan, Proc. Phys. Soc. **83**, 662 (1964).
[7] H. T. Davis, S. A. Rice and L. Meyer, J. Chem. Phys. **37**, 2470 (1962).
[8] L. Meyer, H. T. Davis, S. A. Rice and R. J. Donnelly, Phys. Rev. **126**, 1927 (1962).
[9] J. Levine and T. M. Sanders, Phys. Rev. Letters **8**, 59 (1962).
[10] W. T. Sommer, Phys. Rev. Letters **12**, 1227 (1964).
[11] M. A. Woolf and G. W. Rayfield, Phys. Rev. Letters **15**, 235 (1965).
[12] C. G. Kuper, Phys. Rev. **122**, 1007 (1961).
[13] J. Jortner, N. R. Kestner, S. A. Rice and M. H. Cohen, J. Chem. **43**, 2614 (1965).
[14] K. Hiroike, N. R. Kestner, S. A. Rice and J. Jortner, J. Chem. Phys. **43**, 2625 (1965).
[15] A. M. Tyndall and C. F. Powell, Proc. Roy. Soc. (London) **A129**, 162 (1930).
[16] F. Reif and L. Meyer, Phys. Rev. **119**, 1164 (1960).
[17] The Po^{210} α-particle source was prepared for us by Dr. Richmond of Monsanto Corporation, Nuclear Sources Department, Dayton, Ohio.
[18] R. Gomer, *Field Emission and Field Ionization, Harvard Monographs in Applied Science, No. 9* (Harvard University Press, Cambridge, Massachusetts, 1961).
[19] We are indebted to Dr. Lanny Schmidt and Bret Halpern for assistance in the preparation and use of field emission tips.
[20] R. Henson, Phys. Rev. **135**, 1002 (1964).
[21] B. Halpern and R. Gomer, J. Chem. Phys. **43**, 1069 (1965).

TABLE I. Grid spacings.

Grid pair	Spacing—system 1 (mm)	Spacing—system 2 (mm)
SA	1.66	1.08
AB	13.23	12.69
BB′	1.51	1.33
B′D	3.44	3.27
DC	3.19	3.40

in Fig. 1. The dc biases to all the grids were derived from a battery pack and applied according to the circuit diagram shown in Fig. 1. In addition, two square-wave potentials, identical in frequency but 180° out of phase with respect to each other, were applied at grids S and B′. The net result is that the grid pairs SA and BB′ behave as electrical shutters which synchronously open and close with the frequency of the applied square wave. The varying potential profile corresponding to this gating action is shown in Fig. 2. The open phase of the pair of shutters is represented by the potential profile given by the solid-line configuration in Fig. 2, the closed phase by the dashed-line configuration.

It is clearly shown in the Appendix that frequencies at which the peaks in the collector current occur in Fig. 3 are directly related to the mean time T_0 required for the electrons to drift across the main drift space AB between shutters SA and BB′ under the influence of a constant electric field strength, E, which is determined by the measured grid spacings (given in Table I) and the dc voltages applied to the grids. The mean drift velocity for the electrons is given by the distance AB divided by the mean drift time T_0. This mean drift velocity v_d divided by the strength of the *applied* electric field, is the electron mobility μ by definition.

The applied square wave is derived from the output of a Hewlett-Packard model 211A square-wave generator (1 to 10^6 cps) and further amplified. The output frequency was calibrated against a Hewlett-Packard model 5245L electronic counter. The frequency of the square-wave generator is stable to within 1%, and the wave-form distortion is less than 1%. The electron collector current (10^{-11} to 10^{-13} A) was measured with a Cary model 31 vibrating reed electrometer. All grid potentials were derived from 90 and 300 V batteries, the potentials of which are subdivided by ten-turn Beckman Helipots (500 kΩ wire wound potentiometers) and measured with a Hewlett-Packard model 412A dc vacuum tube voltmeter (maximum reading error is 1% on any range).

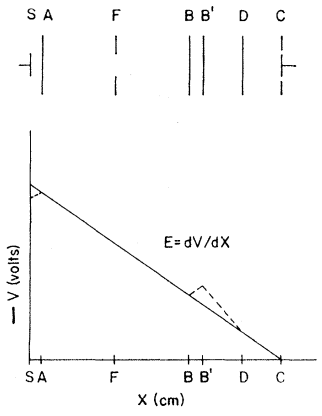

FIG. 2. The potential across the grid system as a function of distance from the electron source S. The solid line represents the potential distribution when the electrical shutters SA and BB′ are open. The dashed lines indicate the modification of the potential in the shutter spaces when the shutters are in their closed phase. The grid spacings shown in this figure are in the same ratio to one another as the grid spacings of the apparatus.

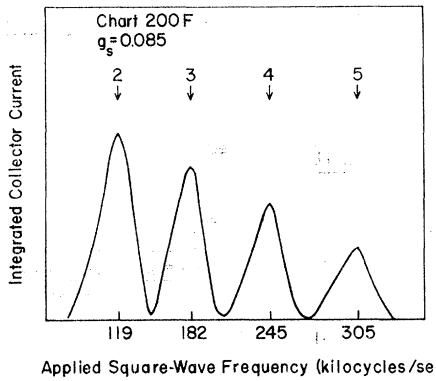

FIG. 3. Experimental current versus electrical shutter frequency for liquid argon ($p=7$ atm, $T=90.1$°K, $E=-200$ V/cm, Chart 200F). The numbers and arrows above the peaks indicate the order of the harmonic. The first peak is not shown since the frequency was swept at a much slower rate on a different frequency range. The value of g_s is 0.0851. The relative amplitudes predicted by Eq. (26) are

$$(A_2:A_3:A_4:A_5)_T = (3.2:2.5:1.7:1)$$
$$(A_2:A_3:A_4:A_5)_{exp} = (2.6:2.1:1.6:1)$$

The last line gives the ratio of the amplitudes of the experimental peaks. The asymmetry factor, χ, predicted on the basis of the analysis given in the appendix, is $1+2g_t=1.17$. Experimentally, this factor is observed to be 1.23 (from the third harmonic in this recording).

The grids are 20-mil phosphor bronze rings (o.d.=1 in., i.d.=7/16 in.), to which a flat copper mesh (0.0015 in. thick, 80 lines per in., 85% open area) is soldered.[22] These grids are gold plated and separated by three sets of nylon spacers and support rods.

The grid spacings given in Table I are the averages of measurements taken in three directions 120° apart. The deviations of the grid spacings measured in any one of these three directions (by a traveling telescope) from the mean grid spacings never exceeded 2%. For the main drift space AB, the deviation from the mean was less than 0.5%.

A schematic diagram of the cryostat used in this experiment is shown in Fig. 4. The cell (a) was immersed in a refrigerant bath (b). The gas to be liquefied was introduced via the stainless-steel capillary (c) from the

[22] This copper mesh is obtained from Buckbee Mears, St. Paul, Minnesota.

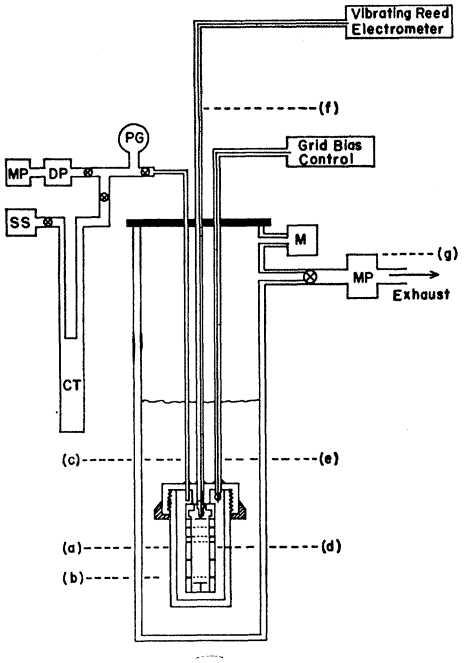

FIG. 4. Schematic diagram of the cryostat and its associated external connections during an experimental run. The essential parts of the system are described in the text. Refer to Fig. 1 for more details on the electronic connections. The symbols are: *MP*=mechanical pump, *DP*=liquid-nitrogen-baffled diffusion pump, *PG*=*USG* pressure gauge, *M*=manometer, *SS*=stainless-steel gas storage cylinders, *CT*=activated cocoanut-charcoal trap.

stainless-steel storage bombs (SS) into which the purified gases are pressurized between experimental runs by the *cryopumping* technique. The cold trap (CT) through which the gas flows on route to liquefaction is an activated charcoal trap cooled to dry ice temperature. The experimental chamber may be evacuated via a liquid-nitrogen-baffled oil-diffusion pump (DP) before each run. The pressure on the liquid in the experimental chamber is measured by a U. S. super gauge (PG). The potentials were applied to the grid system (d) via vacuum-tight coaxial leads (e). The electron current to the collector C was transmitted to the electrometer preamplifier head by the vacuum-tight coaxial line (f). The refrigerant bath could be lowered in temperature by pumping with a mechanical pump (g). The temperature of the bath is derived from its vapor pressure, as measured by the mercury manometer (M). The temperature was checked with a calibrated thermocouple immersed in the bath adjacent to the cell.

This thermocouple was calibrated at 33 points in the temperature range from the triple point of nitrogen to room temperature against a National Bureau of Standards calibrated platinum resistance thermometer.[23] The refrigerant baths were oxygen (84–90°K), methane (90–111.6°K),[24] ethane (125–185°K),[25] carbon tetrafluoride (112–145°K),[26] fluoroform (180–193°K),[26] and Freon-22 (190–232°K).[26] The pressure of the liquid argon was measured with a U. S. super gauge [6-in. dial face, 20 to 2000 psi (absolute)] which was calibrated against a calibrated Heise gauge for which the maximum error is specified by the manufacturer to be 3 psi (absolute).[23] The maximum reading error on the U. S. super gauge is 4 psi (absolute).

The precision of the measured electron mobilities is estimated to be $\pm 3\%$. This estimate is confirmed by the tabulated deviations about the mean of the experimental observations.

III. PURIFICATION OF ARGON AND KRYPTON

Extreme purity of the argon or krypton sample is essential to the success of this experiment. In fact, Swan[27] has estimated, from electron attachment coefficient measurements in liquid argon, that, at electric field strengths of 100 to 200 V/cm, the oxygen impurity content must be less than one part in 10^9, in order to observe the drift velocities of free electrons and not negative ions as observed by Davis, Rice, and Meyer.[28]

Commercial argon was passed through 45 g of activated cocoanut charcoal[29] contained in a stainless-steel, high-pressure cold trap immersed in a dry ice-acetone mixture. This cold trap was installed in the high-pressure line between the stainless-steel storage bombs and the cryostat, as shown in Fig. 4. The charcoal was activated prior to each run by heating the stainless-steel walls of the trap to a faint red glow and simultaneously pumping on the trap with a liquid-nitrogen-baffled oil-diffusion pump to reduce the pressure to 4×10^{-6} mm Hg or less. The trap was pumped under these conditions for 45 min to 1 h. After this thorough out-gassing of the trap, it was filled with argon gas to a slight overpressure and cooled down to dry ice temperature.

The cell was pumped down to about 10^{-4} mm Hg and flushed four times with argon gas which had passed through the trap. After each flushing, the cell was pumped down again to 10^{-4} mm Hg. The cell was then immersed in the refrigerant and the argon liquefied in the cell at a flow rate of approximately four liters of gas (STP) per minute.

The appropriate voltages were then applied to the grids to maintain a field strength of -100 V/cm across

[23] L. D. Ikenberry and S. A. Rice, J. Chem. Phys. **39** 1561 (1963). This reference describes the calibration of the thermocouple.

[24] G. T. Armstrong, F. G. Brickweide, and R. B. Scott, J. Natl. Bur. Std. **55**, 42 (1955).

[25] *Thermodynamic Functions of Gases*, edited by F. Din (Butterworth Scientific Publications, Ltd., London, 1956), Vols. 1 and 2.

[26] The thermodynamic data for the Freons may be obtained from the Freon Products Division, E. I. Dupont de Nemours and Company, Wilmington, Delaware.

[27] D. W. Swan, Proc. Phys. Soc. (London) **82**, 74 (1963).

[28] H. T. Davis, S. A. Rice, and L. Meyer, J. Chem. Phys. **37**, 2470 (1962).

[29] C. L. Mantell, *Industrial Carbon* (D. Van Nostrand Company, Inc., New York, 1946), p. 148.

TABLE II. Argon data.

T(°K)	p(atm)	E(V/cm)	n	$\langle\tilde{\mu}\rangle$ cm²/V/sec	Maximum deviation +	Maximum deviation −
90.1	6.0	−50	2	470	5	5
90.1	6.0	−100	2	470	5	5
90.1	6.0	−100	2	475	2	2
90.1	12.2	−100	2	442	13	13
90.1	12.5	−100	3	478	4	4
90.1	24.8	−100	4	474	5	7
90.1	36.7	−100	3	469	4	8
90.1	49.0	−100	3	448	12	12
90.1	56.5	−100	4	436	4	5
90.1	72.3	−100	6	440	14	7
111.5	6.0	−100	2	290	2	3
111.5	7.5	−100	3	290	6	6
111.5	12.5	−100	3	289	15	11
111.5	24.8	−100	3	317	9	8
111.5	26.4	−100	3	293	1	1
111.5	36.9	−100	4	312	16	9
111.5	36.9	−100	2	305	3	3
111.5	39.6	−100	3	308	3	3
111.5	47.6	−100	3	321	7	5
111.5	49.5	−100	3	314	0	0
111.5	56.1	−100	4	309	0	0
123.4	103.4	−100	3	350	5	8
126.6	96.0	−100	5	340	2	2
129.9	89.2	−100	3	337	0	0
130.8	90.3	−100	2	340	2	2
132.0	78.5	−100	1	338		
133.4	70.8	−100	2	342	0	0
135.3	56.5	−100	1	351		
141.6	57.5	−100	4	417	6	8
142.3	48.4	−100	1	440		
142.6	49.0	−100	1	445		
142.8	49.4	−100	1	449		
143.1	50.2	−100	1	452		
143.6	41.3	−100	2	491	3	3
144.1	42.6	−100	2	503	2	2
145.0	39.9	−100	3	562	10	15
145.0	45.3	−50	1	810		
145.0	45.3	−100	2	523	8	8
145.0	45.3	−150	2	383	1	1
145.0	49.6	−100	4	522	6	6
145.0	57.0	−100	4	487	8	12
145.0	68.7	−100	1	425		
145.0	72.8	−100	4	454	1	1
145.0	85.7	−100	4	440	6	4
145.0	94.1	−100	5	426	8	8
85.0	6.0	−125	5	434	20	15
85.0	6.0	−150	6	456	8	20
85.0	6.0	−175	3	444	8	9
85.0	6.0	−200	5	433	14	11
85.0	14.6	−200	3	458	4	2
90.1	6.9	−150	3	363	9	11
90.1	6.9	−200	6	368	16	16
90.1	7.1	−125	3	352	26	14
90.1	7.1	−150	3	358	1	1
90.1	7.1	−175	3	369	5	9
95.0	6.0	−150	2	381	8	8
95.0	6.0	−200	4	374	3	3
100.3	7.1	−100	3	332	7	4
100.3	7.1	−150	3	343	2	2
100.3	7.1	−200	4	343	2	2
100.3	37.1	−200	1	352		
100.3	70.1	−200	3	366	8	18
100.3	93.6	−200	4	371	3	3
105.5	8.3	−125	5	275	6	6
105.5	8.3	−150	5	284	7	7
105.5	8.3	−175	3	287	6	3
105.5	8.3	−200	5	293	9	7
105.3	9.4	−200	3	288	5	2
105.3	27.2	−200	3	317	18	9
105.3	38.4	−200	3	317	11	11
105.3	67.2	−200	4	316	5	5
105.3	90.2	−200	3	364	7	7
105.3	95.3	−200	4	327	1	1
111.5	6.1	−200	4	276	5	2
111.5	10.3	−175	3	226	9	11
111.5	10.3	−200	5	225	5	7
111.5	44.9	−200	4	293	6	6
111.5	86.8	−200	4	308	2	2
111.5	91.7	−150	3	309	13	13
111.5	91.7	−175	3	325	3	5
111.5	91.7	−200	3	313	1	1

the cell. The current collected at C for this field strength was approximately 10^{-12} A. This field was maintained for about 2h to electrolytically remove trace amounts of electron-trapping impurities, such as oxygen (electron affinity=+0.44 eV), remaining in the argon after the prepurification process. At the end of this 2-h period, the collector current had usually increased by an order of magnitude or more, indicating the appearance of a charge carrier of large drift velocity. Under these conditions, if the potential to any grid was set to zero, the current immediately decayed with no apparent delay time. This is a check for the presence of the high-speed species (the electron). Prior to the 2-h electrolysis period, this check shows a 5- to 20-sec delay in the initial decay of the collector current after one of the grid potentials has been zeroed (negative ions).

The krypton gas used in these experiments was previously purified by Dr. H. T. Davis.[30] The Matheson Research Grade krypton was purified by passing it through an activated copper column at approximately 300°C for oxygen removal and also a titanium column at approximately 500°C for nitrogen removal. The purified gas was stored in 500-cc Hoke spun stainless-steel cylinders. The bombs were connected via a stainless-steel capillary to one side of a high-pressure needle valve and to a USG pressure gauge (3-in. dial face) which reads from 0–3000 psi. The other end of this needle valve was connected via a detachable O-ring connection to the high-pressure manifold. These bombs were filled using conventional cryopumping techniques.

IV. EXPERIMENTAL RESULTS

The liquid-argon data are displayed in Table II and the liquid-krypton data in Table III. The apparent electron mobility $\tilde{\mu}$ which is merely the electron drift velocity divided by the *applied* electric field strength E for *any* value of E (the *mobility* μ is only defined for those values of E satisfied by the relation $v_d=\mu E$), is

[30] H. T. Davis, S. A. Rice, and L. Meyer, J. Chem. Phys. 37, 947 (1962).

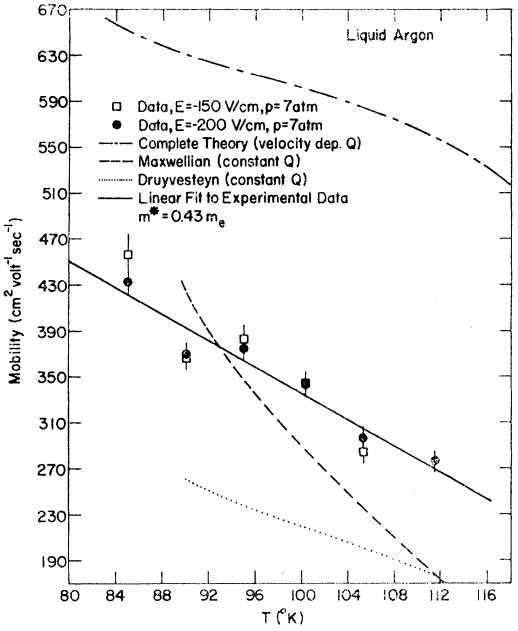

FIG. 5. Electron mobilities in liquid argon as a function of temperature. The dashed line is drawn through points calculated from Eq. (19) (velocity averaging over the Maxwellian distribution). The dotted line represents values calculated from Eq. (22) (velocity averaging over the Druyvesteyn distribution). The mixed dashed and dotted line represents values calculated by numerical integration of Eqs. (6), (7), and (9). All the calculations were performed using the effective mass ($m^*=0.43\ m_e$, and m_e is the free electron mass) obtained from the exciton spectra of solid argon [G. Baldini, Phys. Rev. **128**, 1562 (1962)].

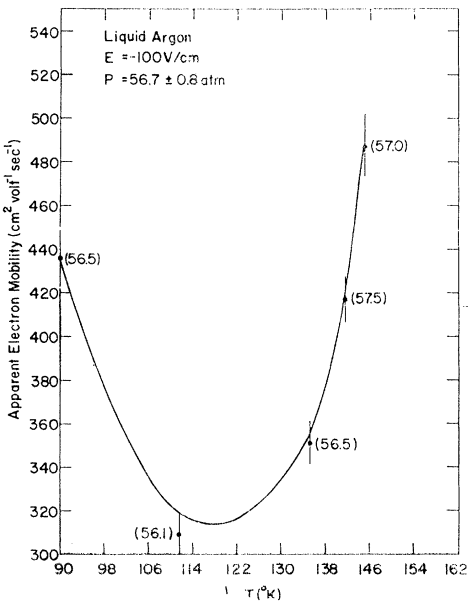

FIG. 6. Apparent mobility of electrons in liquid argon as a function of temperature at a pressure of 57.0±0.5 atm and an electric field strength of −100 V/cm. The pressure reading for each point given in atmospheres is written within the parentheses adjacent to that point.

TABLE III. Krypton data.

T(°K)	p(atm)	E(V/cm)	n	$\langle\tilde{\mu}\rangle(10^{-3})$ cm²/V/sec	Maximum deviation +	−
120.4	4.7	−100	3	1.31	3	4
120.2	9.8	−100	2	1.29	0	0
120.2	15.1	−100	2	1.29	3	3
120.2	20.1	−100	4	1.31	3	5
120.1	25.7	−100	2	1.26	3	3
120.2	29.9	−100	3	1.32	2	3
120.6	28.7	−100	3	1.29	3	4
122.7	1.6	−100	3	1.28	0	0
124.0	1.6	−100	2	1.34	2	2
129.3	15.1	−100	2	1.27	1	1
129.4	32.8	−100	4	1.27	2	2
131.7	24.8	−100	3	1.31	1	2
132.4	12.1	−100	1	1.32		
132.7	4.4	−100	1	1.30		
139.6	4.4	−100	9	1.43	3	2
139.5	12.0	−100	3	1.45	1	1
139.6	15.0	−100	4	1.41	0	0
139.5	19.3	−100	3	1.44	0	0
139.4	25.2	−100	5	1.42	2	2
139.7	33.2	−100	4	1.40	0	0
145.5	32.9	−100	5	1.40	0	0
151.4	10.8	−100	4	1.60	3	2
152.1	15.6	− 50	4	2.29	5	8
151.6	15.1	−100	5	1.56	1	1
151.7	15.3	−150	5	1.16	0	1
151.8	19.9	−100	5	1.52	3	3
151.6	25.9	−100	5	1.55	0	1
151.4	27.8	−100	5	1.51	1	2
151.9	32.5	−100	5	1.58	3	4
152.3	12.4	−100	5	1.57	1	2
159.8	29.2	−100	4	1.68	3	3
160.0	15.0	−100	3	1.73	1	2
160.1	25.6	−100	3	1.78	2	5
160.0	32.5	−100	6	1.71	3	3
166.2	21.8	−100	6	1.93	2	3
165.6	25.5	−100	3	1.92	3	4
165.5	28.4	−100	4	1.92	3	4
165.4	33.2	−100	4	1.93	1	1
169.3	25.6	−100	3	2.00	3	2
169.8	28.7	−100	5	2.12	2	2
169.8	32.4	−100	6	2.08	5	7
169.4	30.5	−100	3	1.97	3	5
170.6	14.8	−100	3	2.08	2	2
170.9	25.3	−100	3	2.09	1	1
170.5	31.6	−100	4	2.05	5	1
179.3	25.4	−100	3	2.18	2	2
180.3	28.6	−100	4	2.37	0	0
180.1	32.9	− 50	3	3.61	2	4
179.9	32.9	−100	4	2.35	2	2
180.0	33.0	−150	4	1.70	1	1
182.8	25.9	−150	3	1.78	2	1
183.1	32.9	−150	5	1.75	2	1
184.5	25.3	−100	4	2.20	2	2
184.8	25.0	−100	4	2.06	1	2
184.5	28.4	−100	4	2.26	2	1
184.8	29.7	−100	3	2.24	7	8
184.5	32.7	−100	5	2.32	1	2
184.8	31.3	−100	5	2.20	3	1
200.8	62.6	−100	2	1.12	1	1
200.9	69.2	−100	3	1.31	1	1
139.6	28.4	−100	3	1.40	0	0

recorded in these two tables as an average value $\langle\tilde{\mu}\rangle$ over the number of experimental observations n. The maximum negative and positive deviations for each set of experimental observations, over which the average is taken, are also given in their respective columns. In the tabulation of our data, we have chosen to present the *apparent electron mobility* rather than the electron drift

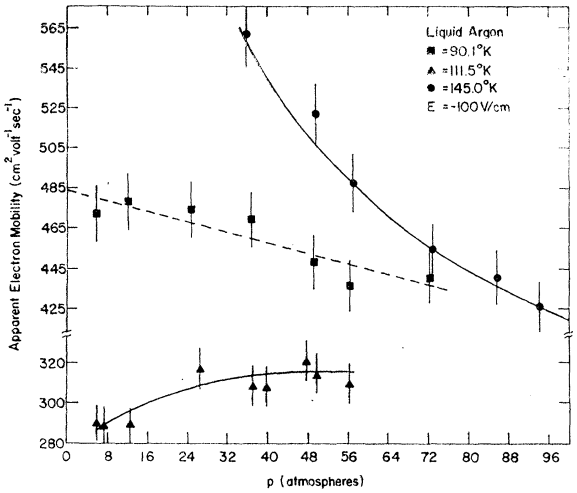

FIG. 7. Apparent mobility of electrons in liquid argon as a function of pressure. All points were measured at a constant electric field strength of −100 V/cm.

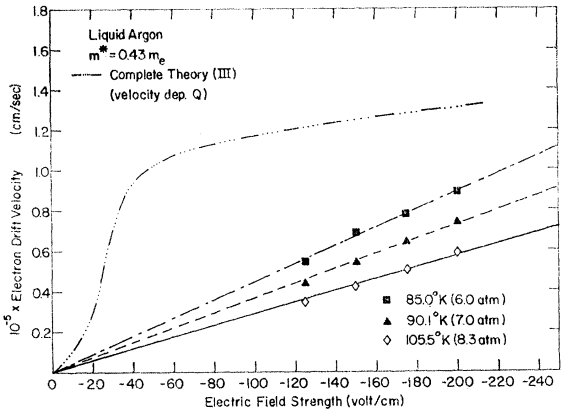

FIG. 9. Electron drift velocities in liquid argon as a function of electric field strength. Notice that the drift velocities appear to be linear in the electric field strength and that the straight lines extrapolate through the origin. The curved line (——···——) in the figure is drawn through points calculated from Eqs. (6), (7), and (9), using a(0), an effective mass of 0.43 of the free-electron mass, and the energy-dependent cross section data of Frost and Phelps (Ref. 3).

velocity. The latter can always be obtained by multiplying $\tilde{\mu}$ by the electric field strength E. There is a deliberate break in the tabulation of Table II in order to separate the data which were taken with the apparatus using a Po^{210} alpha-emitting source and the data which were taken with the apparatus using the tungsten field emission tip as the electron source (this data follows the break). All of the data given in Table III were taken using the Po^{210} source.

In Fig. 5 we display the experimental temperature dependence of the electron mobility in liquid argon in that temperature range in which the electron drift velocity is linear in the electric field strength. It should be noticed that in this temperature range the mobility decreases with an increase in temperature, as elementary theories predict. In Fig. 6 we display the complete temperature dependence of the apparent electron mobility in liquid argon. The anomalous minimum in the temperature dependence is striking. The data appear to

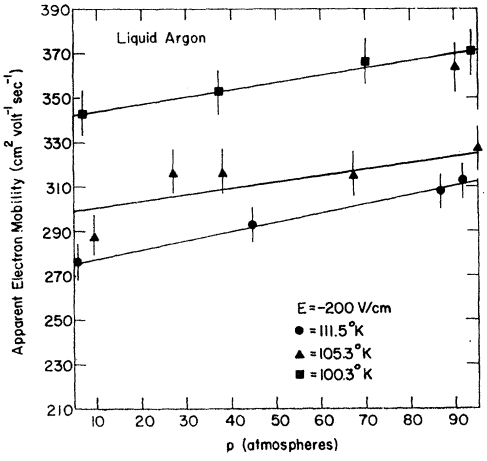

FIG. 8. Apparent electron mobility in liquid argon as a function of pressure. All points were measured at a constant electric field strength of −200 V/cm.

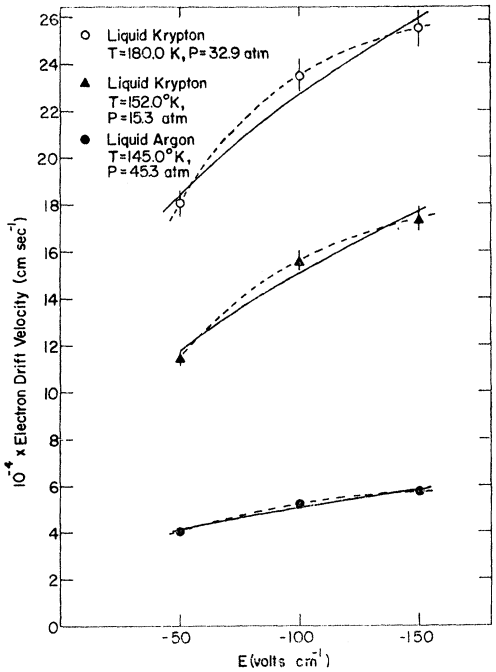

FIG. 10. Electron drift velocities in liquid argon and in liquid krypton as a function of electric field strength. We have fitted the experimental points to polynomials of the form

$$v_d = a + bE^{1/2} \quad \text{(a)}$$

$$v_d = c + dE^{1/2} + fE. \quad \text{(b)}$$

The solid curves in the figure represent Eq. (a), and the dashed curves represent Eq. (b). The numerical coefficients a–f were evaluated for each curve by least-squares polynomial fitting.

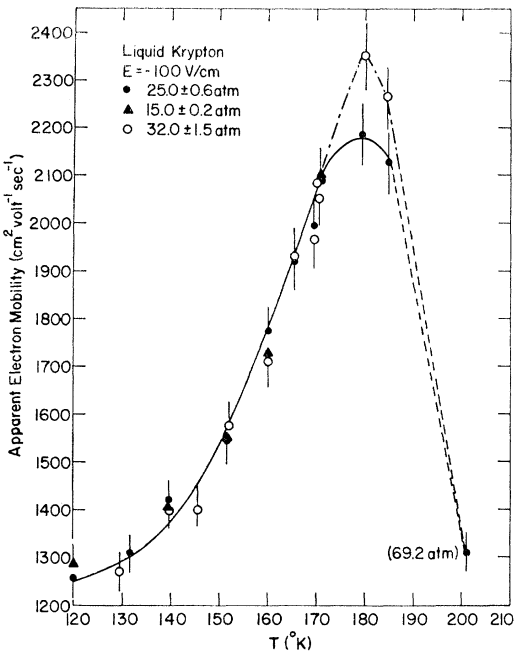

FIG. 11. Apparent electron mobility in liquid krypton as a function of temperature. All points are measured at a constant electric field strength of −100 V/cm. Notice the point at 200.9°K was measured at a pressure of 69.2 atm. We display this point to indicate a possible maximum in the temperature dependence of the apparent electron mobility in liquid krypton. This is valid since the liquid krypton data is insensitive to pressure (see Fig. 12.)

show a direct correlation between the onset of the nonlinear dependence of the electron drift velocity on the electric field and the change in sign of the slope of the apparent electron mobility versus temperature curve shown in Fig. 6. Since we have data on the electric field dependence of the drift velocity for only one temperature in the immediate vicinity of this minimum, no definite conclusion on this possible correlation can be drawn.

The pressure dependence of the apparent electron mobilities in liquid argon are given in Figs. 7 and 8.

The electron drift velocity in liquid argon as a function of electric field strength is displayed in Fig. 9. The three experimental isotherms plotted in this figure are linear and intercept the origin. In contrast to Fig. 9, we find that the electron drift velocities displayed in Fig. 10 are definitely nonlinear in the electric field strength. The solid lines in Fig. 10 are least-squares fits of the experimental points to a polynomial of the form

$$v_d = a + bE^{1/2}, \tag{1}$$

and the dashed lines are least-squares fits to a polynomial of the form

$$v_d = c + dE^{1/2} + fE, \tag{2}$$

where v_d is the electron drift velocity, E is the electric field strength, and the other letters are numerical coefficients. Equation (1) is of interest since this is the functional form predicted by Wannier[31] for electron drift velocities in gases in the high-field limit $(e\Lambda E \gg (m_e/M)kT$, where e is the electronic charge, Λ is the mean free path for the electron, kT is the thermal energy, m_e is the electron mass, and M is the mass of the fluid atom). Equation (2) is a combination of Eq. (1) with the functional form expected in the zero-field limit, viz., $v_d = fE$. The excellent fit of the experimental points to the functional form of Eq. (2) suggests that the data is in the complicated intermediate range of electric field strengths.

The temperature dependence of the apparent electron mobility in liquid krypton is given for several constant pressures and for a constant electric field strength of −100 V/cm in Fig. 11. All points fall approximately on the same curve except between 180 and 190°K. It is very difficult to purify the gases at temperatures above dry ice temperature, and for this reason we have successfully obtained only one data point above 190°K. This one point is very interesting in that it appears to show an anomalous maximum in the temperature dependence of the apparent electron mobility in liquid krypton. Obviously, the exact shape of the curve is uncertain above 190°K, and this is indicated in Fig. 11 by the dashed-line extrapolations to the curves.

In Fig. 12 we show the pressure dependence of the apparent electron mobility in liquid krypton. In the range of pressures studied, the mobility appears to be independent of pressure in liquid krypton.

V. THEORETICAL CONSIDERATIONS

The scattering of an electron by a dense assembly of atoms involves a complex many-body interaction and evokes problems not ordinarily posed in the more usual applications of scattering theory. Perhaps the most difficult of these problems is caused by the nonexistence of true asymptotic states for the scattering process. That is, since the electron is in the medium and has a wavelength comparable with or greater than the average intermolecular spacing, the electron is always in interaction with some atoms. Under these conditions, there is no meaning to precollision and postcollision asymptotic states in which the electron is considered to be out of the range of interaction of the scattering center.

Stated in these terms, the situation appears hopelessly complex. However, by exploitation of an analogy and with the use of a dash of intuition, it is possible to construct a physically reasonable analysis in the limit that the scattering of an electron by any one atom is weak. Our analysis is based on the assumption that it is possible to define an effective electron-atom scattering cross section in the dense liquid. Because of the long range of the polarization interaction, which contributes

[31] G. Wannier, Bell System Tech. J. 32, 170 (1953).

to the free atom–electron scattering cross section, it is necessary to allow for the reduction in the induced dipole moment of an atom due to interactions with the induced dipole moments of the surrounding atoms. For a localized charge this screening can be calculated in the self-consistent-field (SCF) approximation.[32] The result is a screening function which causes maximum screening at an electron-atom distance corresponding to the first peak in the radial distribution function, has an asymptotic value of 0.78 as $R \rightarrow \infty$, and, properly, gives no screening inside the atom. The details of this analysis will be published elsewhere.[32] For our purposes, it is sufficient to note that, with the SCF screening function and assuming no overlap of the short-range electron-atom interactions, the influences of the fields generated by the surrounding atoms are properly included in an effective single atom-electron scattering cross section.

In order to develop a simple analysis, it is also necessary to assume that the electron in Ar does not alter the local structure of the liquid. Because the charge of the electron is not concentrated at a point but is spread over a volume determined by the electron wavelength, this is a reasonable approximation. A direct implication of this assumption is that the Wigner function, or the density matrix, for the system of N atoms plus one electron, becomes a product of the function for the N atoms isolated from the electron and the function for the electron.

To derive a transport equation for the system under discussion, we start with the analysis of Davis, Hiroike and Rice.[33] The equation for the full Wigner function may be contracted to yield an exact equation for the time and phase-space variation of the electron Wigner function in terms of an integral over the joint electron-atom Wigner function (which will be factorizable) and the interaction. To obtain the usual Boltzmann equation, it is necessary to assume that the electron-atom system has well-defined precollision and post-collision states. While this assumption is valid in the dilute gas, it cannot be correct in the dense liquid, as mentioned above.

The theory of light scattering suggests, by analogy, a method for handling this problem. The contracted form of the equation for the full Wigner function can be displayed in another form equivalent to the one described above. In this form the time and phase-space dependence of the electron Wigner function is represented in terms of the full Wigner function, integrated over the coordinates and momenta of all the atoms in the liquid. Then the simultaneous interactions of the electron and all atoms concerned are explicitly, rather than implicitly, displayed. Let the electron be represented by a wave packet. Further, assume that the wave packet does not spread much as the result of a single scattering. Then it is possible to reconstruct the

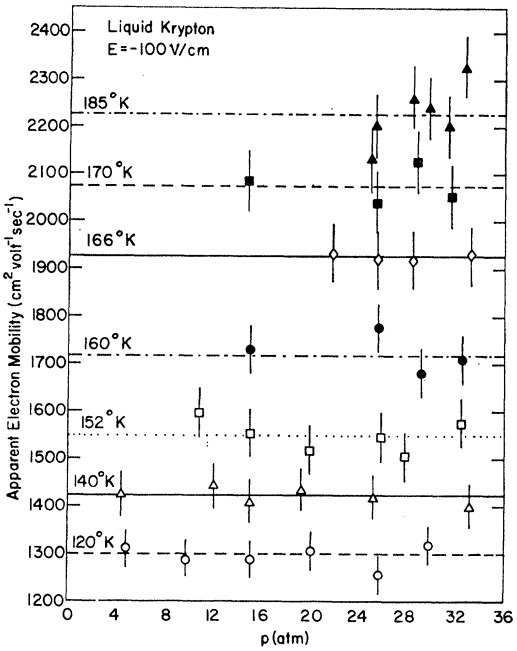

FIG. 12. Apparent electron mobility in liquid krypton as a function of pressure at a constant electric field strength of −100 V/cm.

scattering of the wave packet by decomposing it into a superposition of plane waves, examining the scattering of each plane wave, and resynthesizing the scattered wave packet from the scattered plane waves. In the description of light scattering from a liquid, the wavelength of the radiation is large relative to the interatomic spacing, with the result that a single scattering event involves the superposition of scattered waves, with their phase relations, from many scattering centers. Because the scattering is weak, the net effect is to simply replace the free atom-radiation scattering cross section by an effective cross section per atom, which involves: (a) the change in effective atomic properties due to interactions in the medium (local field effects); and (b) the structure factor of the liquid.

The ansatz we suggest, then, is that the simultaneous interaction of the electron with many atoms and the implicit lack of pre- and postcollision states are adequately approximated by use of an effective electron-atom scattering cross section which is the product of the liquid-structure factor, $a(\mathbf{K})$, and the locally modified electron-atom scattering cross section. With this ansatz, the integral over the full Wigner function need no longer be considered. Instead, we may use the reduced joint electron-atom Wigner function. Use of the ansatz on scattering then leads to a generalized Boltzmann equation, with electron-atom cross section explicitly including the interference generated by other atoms in the fluid through the liquid-structure factor.

The reader will note that the suggested form of the modified Boltzmann equation is that which would be

[32] J. Lekner, (private communication).
[33] H. T. Davis, K. Hiroike, and S. A. Rice, J. Chem. Phys. 43, 2633 (1965).

expected from an analysis of the mean free time by the methods of Ziman.[34,35] We have given the argument presented above because the mean-free-time theory assumes that a Boltzmann equation exists, whereas we wish to examine whether it does exist, and in what form, for our case. For electrons in metals, the Fermi energy is sufficiently large, the electron wavelength sufficiently small, and the overlapping of atomic fields sufficiently small, that the problem of defining the scattering process is much less complex than for an electron in Ar.

Having argued that a suitable approximation to the electron scattering problem is provided by a modified Boltzmann equation, we may now take over the results of the extensive investigations of Chapman and Cowling[36] and of Morse, Allis and Lamar.[37] These workers have solved the ordinary dilute-gas Boltzmann equation for electrons in steady-state motion under the influence of an electric field. In particular, they assume that: (1) Only elastic scattering need be considered; (2) the electron singlet distribution function is homogeneous; and (3) the surrounding medium is always at equilibrium. The first assumption is certainly valid in our systems, as is the second because of the small concentration of electrons. Indeed, our electron concentration is so small that electron-electron interactions are completely negligible ($\ll kT$). The third assumption is also valid, because one particle can only lead to a change in the singlet distribution function of N surrounding particles of the order of N^{-1}.

It is clear that the three assumptions cited are completely consistent with the modified Boltzmann equation suggested (using words only) herein, since this equation differs from the dilute-gas Boltzmann equation only in the form of the scattering cross section. What, then, are the principal features of the solution of the modified Boltzmann equation?

The electron velocity distribution function may be expanded in terms of the ratio v_x/v, where v_x is the velocity component in the direction of the electric field and v is the total velocity of the electron. The expansion cited has the following form:

$$f=f_0+\left(\frac{v_x}{v}\right)f_1+\left(\frac{v_x}{v}\right)^2 f_2+\cdots. \tag{3}$$

Morse *et al.*[37] have shown that at the mean electron energy, f_2/f_1 is proportional to $(m_e/M)^{1/2}$, where m_e is the mass of the electron and M is the mass of an atom of the fluid. Thus, terms of order higher than f_1 may be neglected. It is then possible to show that (Chapman and Cowling[36])

$$-[1+\epsilon\alpha(\epsilon)]\frac{\partial f_0}{\partial\epsilon}=\frac{\epsilon}{kT}\alpha(\epsilon)f_0(\epsilon), \tag{4}$$

where $\epsilon(=\frac{1}{2}m_e v^2)$ is the kinetic energy of the electron, k is Boltzmann's constant, T is the absolute temperature, and $\alpha(\epsilon)$ is defined by

$$\alpha(\epsilon)=\frac{6m_e}{M}\left[\frac{\rho_N Q_m{}^L(\epsilon)}{eE}\right]^2 kT, \tag{5}$$

with ρ_N the number density of the fluid, $Q_m{}^L(\epsilon)$ the energy-dependent momentum-transfer cross section for the liquid phase, e the electronic charge, and E the electric field strength. As already remarked, the characteristics of the dense medium are introduced into the theory through the structure of $Q_m{}^L(\epsilon)$. Equation (4) may be integrated to give[36,37]

$$f_0(\epsilon)=\exp\left[-\frac{1}{kT}\int_0^\epsilon\frac{\epsilon'\alpha(\epsilon')d\epsilon'}{1+\alpha(\epsilon')\epsilon'}\right]. \tag{6}$$

It may also be shown[37] that

$$f_1=-\left[\frac{eE}{\rho_N Q_m{}^L(\epsilon)}\right]\frac{\partial f_0}{\partial\epsilon}. \tag{7}$$

The mean energy and the drift velocity of the electron may now be calculated in terms of the expansion functions given by Eqs. (3), (6), and (7), since

$$\bar{\epsilon}=\langle\epsilon\rangle=\frac{4\pi\sqrt{2}}{m_e{}^{3/2}z}\int_0^\infty\epsilon^{3/2}f_0(\epsilon)d\epsilon \tag{8}$$

and

$$v_d=\langle v_x\rangle=\frac{\int_0^\infty v_x(v_x/v)f_1v^2dv}{\int_0^\infty f_0v^2dv}=\frac{4\pi\int_0^\infty\epsilon f_1(\epsilon)d\epsilon}{3(m_e)^2z}, \tag{9}$$

where z is the normalization factor

$$z=\int_0^\infty f_0(v)4\pi v^2dv=\frac{4\pi\sqrt{2}}{(m_e)^{3/2}}\int_0^\infty f_0(\epsilon)\epsilon^{1/2}d\epsilon. \tag{10}$$

The reader should note that we have approximated $v_x{}^2$ by its value for an isotropic velocity distribution $\frac{1}{3}v^2$. Since the ratio of the drift velocity to v is of the order of $(m_e/M)^{1/2}$, this approximation is reasonable.

We must now turn our attention to the evaluation of the elastic-scattering cross section. As already noted, and building on the light-scattering analogy cited, we shall assume that this cross section may be written as the product of the energy-dependent (**K**-dependent) elastic-scattering cross section for an isolated scattering center (argon atom in the gas phase) $Q_m(\epsilon)$ and the liquid structure factor $a(\mathbf{K})$ defined by the following expression[38]

$$Na(\mathbf{K})=|\textstyle\sum_n\exp(i\mathbf{K}\cdot\mathbf{r}_n)|^2, \tag{11}$$

[34] J. M. Ziman, Phil. Mag. 6, 1013 (1961).
[35] N. E. Cusack, Rept. Prog. Phys. 26, 361 (1963).
[36] S. Chapman and T. G. Cowling, *The Mathematical Theory of Nonuniform Gases* (Cambridge University Press, New York, 1939).
[37] P. M. Morse, W. P. Allis, and E. S. Lamar, Phys. Rev. 48, 412 (1935).
[38] G. Fournet and A. Guinier, *Small Angle Scattering of X Rays* (John Wiley & Sons, Inc., New York, 1955).

where $|\mathbf{K}|=(4\pi/\lambda)\sin(\frac{1}{2}\theta)$, λ is the wavelength associated with the incident particle, θ is the angle of deflection, and $\mathbf{r}_n$ is the position vector of the nth atom in a fluid of N particles. This liquid structure factor, $a(\mathbf{K})$, is also related to the radial distribution function, $g(r)$, of the fluid by Fourier transformation,[39,40]

$$a(K)=1+\rho_N\int_0^\infty[g(r)-1]\frac{\sin(Kr)}{Kr}4\pi r^2dr, \quad (12)$$

and in the limit of thermal energies,[41]

$$a(K=0)=\rho_N kT\kappa_T, \quad (13)$$

where κ_T is the isothermal compressibility of the liquid. In this approximation, we write the cross section in the form

$$Q_m{}^L(\epsilon)=Q_m(\epsilon)a(K), \quad (14)$$

where $Q_m(\epsilon)$ is the momentum-transfer cross section for electrons in the gas phase. This implies that the interatomic interactions in the liquid are sufficiently weak to lead, aside from shielding effects, only to negligible changes in the gas-phase momentum-transfer cross section for a single atomic scattering center. If now it is assumed that the cross section is constant and independent of energy, two limiting cases of interest arise:

(a) If the field energy of the electron,

$$[eE/\rho_N Q_m(\epsilon)a(K)],$$

is much less than the thermal energy (kT), and the cross section is constant and independent of energy, we write the zero energy limit for $Q_m{}^L$ given by Eq. (14), i.e., $Q_m(0)a(0)$, and Eqs. (4) and (7) reduce to

$$\frac{1}{f_0}\frac{\partial f_0}{\partial\epsilon}=-\frac{1}{kT} \quad (15)$$

and

$$f_1=\frac{eE}{\rho_N Q_m(0)a(0)}\frac{f_0}{kT}, \quad (16)$$

where f_0 is the Maxwellian distribution obtained directly from Eq. (15). Clearly, to complete the calculation of the drift velocity in this approximation, we must evaluate $Q_m(0)$ and $a(0)$. $a(0)$ is given by Eq. (13). $Q_m(0)$ is determined by a partial wave solution of the Schrödinger equation describing the steady-state scattering of a homogeneous incident beam of noninteracting particles impinging on a single center.

The magnitude of the wave vector, $\mathbf{k}$, for thermal electrons in liquid argon is of the order 6×10^{-2} Å^{-1}, and it is easily established that we need consider only s-wave scattering, described by the phase shift η_0. It is convenient, then, to introduce the scattering length

$$a=\lim_{k\to0}[-(\sin\eta_0)/k] \quad (17)$$

via the relation

$$Q(0)=4\pi a^2, \quad (18)$$

where $Q(0)$ is the total elastic-scattering cross section for $k=0$. Note that in this limit, $k\to0$, corresponding to thermal electrons, $Q(0)$ is independent of velocity.

Assuming that $Q(0)$ is equivalent to $Q_m(0)$, we may use Eqs. (9), (10), (13), (15), (16), (17), and (18) to derive

$$\mu_T=\frac{v_d}{E}=\frac{e}{3\sqrt{2}\pi^{3/2}(kT)^{3/2}\rho_N{}^2(m_e{}^*)^{1/2}\kappa_T a^2}, \quad (19)$$

where μ_T is the electron mobility representing this approximation (electron energies less than thermal).

(b) The second limiting expression for the mobility is obtained if it is assumed that the field energy, $eE/\rho_N Q_m(\epsilon)$, is much greater than the thermal energy. Then $\epsilon\alpha(\epsilon)$ is very small relative to unity and Eqs. (5), (6), and (7) become

$$\frac{1}{f_0}\frac{\partial f_0}{\partial\epsilon}=\frac{-6m_e{}^*}{M}\left[\frac{\rho_N Q_m{}^L(\epsilon)}{eE}\right]^2\epsilon \quad (20)$$

and

$$f_1=\frac{6m_e{}^*}{M}\left[\frac{\rho_N Q_m{}^L(\epsilon)}{eE}\right]\epsilon f_0. \quad (21)$$

Assuming an energy-independent cross section, Eq. (20) is readily integrated to give a Druyvesteyn distribution for f_0. The Druyvesteyn distribution is proportional to $e^{-A\epsilon^2}$.

Substituting this f_0 into Eq. (21), f_1 is obtained. These expressions for f_0 and f_1, along with the energy-independent cross section

$$\rho_N kT\kappa_T 4\pi a^2=Q(0)a(0),$$

may be used to evaluate Eq. (9) with the result

$$\tilde{\mu}_D=\frac{v_d}{E}=\frac{0.248e^{1/2}}{|a|(m_e{}^*M)^{1/4}(kT)^{1/2}\rho_N\kappa_T{}^{1/2}E^{1/2}}. \quad (22)$$

Finally, at the present time, the best approach to the problem, consistent with the assumptions implied when one writes the expression given in Eq. (14), is to use the energy-dependent $Q_m{}^L(\epsilon)$ in Eq. (5) and numerically integrate Eqs. (6)–(10). The results displayed in the columns headed by $\tilde{\mu}$ [Eq. (9)] and $\tilde{\epsilon}$ in Tables IV and V were obtained by numerical integration of Eqs. (8) and (9), replacing $Q_m{}^L(\epsilon)$ by $Q_m(\epsilon)a(0)$. $Q_m(\epsilon)$ was obtained from the tabulated experimental data of Frost and Phelps (see Ref. 3) and the $\kappa=0$ limit of $a(K)$ is given by Eq. (13).

There is a considerable discrepancy[42] between the

[39] N. S. Gingrich, Rev. Mod. Phys. **15**, 90 (1943).
[40] T. Hill, *Statistical Mechanics* (McGraw-Hill Book Company, Inc., New York, 1956).
[41] L. D. Landau and E. M. Lifshitz, *Statistical Physics* (Pergamon Press, Ltd., London, 1959).
[42] A. Rahman, J. Chem. Phys. **42**, 3540 (1965).

TABLE IV. Results of electron-mobility calculations.[a,b]

T(°K)	p(atm)	$\tilde{\mu}_T$[c,d]	$\tilde{\mu}_D$[c,d]	$\tilde{\mu}$ (Eq. 9)[c,d]	$\bar{\epsilon}$[e]	$\tilde{\mu}_+$[c,f]	$\tilde{\mu}_D$[c,f]	$\tilde{\mu}$ (Eq. 9)[c,f]	$\bar{\epsilon}$[g]	$\langle\mu\rangle_{\text{exp}}$[c]
84	0.7			612	0.46			656	0.53	
85	6.0									433
90.1	7.1	280	211	591	0.42	427	260	631	0.49	368
95.0	6.0	226	192			344	236			374
100.3	7.1	188	178	563	0.38	287	219	601	0.44	343
105.3	8.3	155	163			236	200			293
110	6			526	0.32			566	0.39	
111.5	6.1	116	144			177	177			276
120	12			428	0.21			516	0.31	
140	39.5	29	76			44	93.5			
100.3	7.1	188	178			287	219			343
100.3	27.2	199	183			303	225			
100.3	37.1	204	185			311	228			352
100.3	70.1	220	192			335	236			366
100.3	93.6	230	197			350	242			371

[a] All values of $\tilde{\mu}$ correspond to a constant electric field of -200 V/cm.
[b] The energy-dependent cross section used in these calculations was taken from Ref. 3.
[c] All values of $\tilde{\mu}$ are in units of cm^2 V^{-1} sec^{-1}.
[d] These apparent mobility values, $\tilde{\mu}$, were calculated on the assumption of an effective mass, m^*, equal to the free-electron mass, m_e.
[e] The mean electron energies (in eV) tabulated in this column were calculated from Eq. (8) with $m^*=m_e$.
[f] These values of $\tilde{\mu}$ were calculated from the appropriate equations [Eqs. (19), (22), and (11)] assuming $m^*=0.43\ m_e$.
[g] The mean electron energies (in eV) tabulated in this column were calculated from Eq. (8) with $m^*=0.43\ m_e$.

experimental results obtained for $a(K)$ by x-rays[43] and neutron[44] diffraction. For this reason, the full K dependence of $a(K)$ is not included in the calculations tabulated in Tables IV and V, but only its $K=0$ limit [Eq. (13)]. However, we have tested the effect of $a(K)$ on the calculation by using an $a(K)$ function calculated from the Percus-Yevick (PY) equation of state for the hard-sphere fluid.[45,46] The PY equation of state agrees with the experimental equation of state[47] to within 6%, and we would expect similar agreement in $a(K)$. Because of the Ramsauer minimum in $Q_m(\epsilon)$ at about 0.3 eV, the only part of $a(K)$ which affects the numerical integration significantly is the flat part from $K=0$ to $K=0.5$ Å^{-1}. The function $a(K)$ is almost constant in this flat region [equal to $a(0)$]. We have found that the calculated values for the apparent mobility given in Tables IV and V decreases only by about 20% when the full $a(K)$ dependence is used in the calculation.

TABLE V. Field dependence of the electron drift velocity.[a]

E (V/cm)	ϵ (eV) (Eq. 8)	v_d (m/sec)	$\tilde{\mu}$ (Eq. 9) cm^2/V/sec	$\langle\tilde{\mu}_{\text{exp}}\rangle$ cm^2/V/sec
5	0.015	54	1080	
10	0.016	108	1080	
15	0.020	172	1146	
20	0.038	284	1420	
25	0.085	481	1924	
30	0.149	691	2303	
35	0.204	840.5	2401	
40	0.245	931	2328	
45	0.274	987	2193	
50	0.297	1025	2050	
55	0.315	1051	1911	
60	0.331	1073	1788	
100	0.413	1173	1173	
125	0.449	1216	973	434
140	0.468	1239	885	
150	0.480	1253	835	456
175	0.507	1286	735	444
200	0.532	1317	659	433
400	0.687	1487	372	

[a] $\bar{\epsilon}$, v_d, and μ were calculated via Eqs. (8) and (9) for $T=84$°K and $p=0.7$ atm. The energy-dependent cross-section data found in Ref. 3 was modified for these calculations by multiplying by $a(0)$. An effective mass of $0.43m_e$ (m_e is the free-electron mass) was assumed in these calculations.

The reader should note carefully how the mean electron energy in liquid argon *exceeds* thermal energies (kT) at all electric fields in excess of 1 V/cm^{-1} according to the calculations given in Table V [numerical integration of Eq. (8)]. This important result shall be discussed in the next section.

The numerical evaluation of Eqs. (9), (19), and (22) is plotted in Figs. 5, 9, and 13. The "complete theory" designation in these figures is equivalent to the results of the numerical evaluation of Eq. (9).

VI. DISCUSSION

The large magnitudes of the mobilities of the "negative species" in liquid argon and liquid krypton provide sufficient evidence that the "negative species" is an unbound electron. This conclusion is substantiated by a direct comparison between our data and the data obtained by Davis, Rice, and Meyer.[7] The mobilities reported in this paper are approximately five orders of magnitude greater than those observed by Davis *et al.* In fact, Davis, Rice, and Meyer[7] suggested that the

[43] N. S. Gingrich and C. W. Tompson, J. Chem. Phys. **36**, 2398 (1962).
[44] D. G. Henshaw, Phys. Rev. **105**, 976 (1957).
[45] J. K. Percus and G. J. Yevick, Phys. Rev. **110**, 1 (1958).
[46] E. Thiele, J. Chem. Phys. **39**, 474 (1963).
[47] S. A. Rice and J. Lekner, J. Chem. Phys. **42**, 3559 (1965).

negative species they observed was, most likely, the O_2^- ion. With but one exception,[8] excess electron mobilities at the low electric fields used in these experiments have never previously been observed in the liquid state. We should emphasize that we are discussing the motion of *excess* electrons in the liquid. Certainly, the conductivity of alkali-metal liquid-ammonia solutions[1] and the conductivity of liquid metals[34,35] is due to electronic conduction, but the interpretation of the properties of these electrons presents a different problem, since they move in the presence of positive ion cores and are concentrated (10^{15}–10^{22} electrons/cc). The mobilities observed for the negative species in liquid helium I by Meyer, Davis, Rice, and Donnelly[8] are of the order of 10^{-1}–10^{-2} cm^2 V^{-1} sec^{-1}, which is about the same as the mobility of the positive species. However, there are important qualitative differences between the behavior of the mobilities for the positive and negative species with respect to density and pressure variations, and these differences indicate a fundamental difference in the nature of the two species. Meyer, Davis, Rice, and Donnelly[8] claim that the negative species is an electron. Their claim has been strongly supported by recent theoretical calculations[13,14] and experiments.[9–11] Hiroike, Kestner, Rice, and Cohen[14] have recently calculated the free energy of an electron trapped in a "bubble" relative to the free energy of the free state for the electron in the liquid. They find that the electron in the bubble has a lower free energy than the electron in the free state in liquid helium I. In the bubble model, the strong repulsive interactions between the electron and the helium atoms force the creation of a void in the fluid of such a size that a balance is achieved between the repulsive interactions, the increased kinetic energy resulting from its localization within the bubble, and the surface and PV work required to create the void in the fluid. A balance is achieved when the bubble diameter approaches 12.4 Å. A calculation using Stokes' law for the electron-in-the-bubble unit predicts a mobility in good agreement with experiment. Perhaps the strongest evidence in support of the bubble model is provided by the striking experiments of Levine and Sanders.[9] These authors have measured the electron mobility as a function of pressure in helium vapor. At a pressure of approximately $0.7p_s$ (p_s is the saturated vapor pressure of He at 4.2°K), there is a sharp decrease in the mobility (of three to four orders of magnitude) to a value characteristic of the liquid state. This can only be explained by some change in the distribution of the helium atoms around the electron and the subsequent movement of this "structure" as a unit. Sommer's experiment[10] demonstrates that liquid helium acts as an energy barrier of magnitude 1.3 eV for electrons incident to its surface. Woolf and Rayfield have accurately determined this energy barrier to be 1.02 eV as shown by the shift in the response on the incident-photon energy scale for a photoelectric tube filled with liquid helium.[11] This

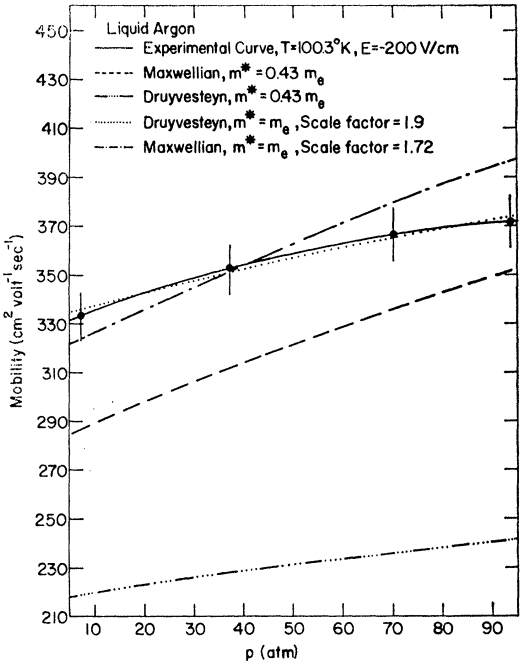

FIG. 13. Electron mobilities in liquid argon as a function of pressure at a constant electric field strength of −200 V/cm and a temperature of 100.3°K. The dashed line is drawn through points calculated from Eq. (19), using an effective mass, m^*, of 0.43 m_e (velocity averaging over the Maxwellian distribution). The line represented by the mixed symbols of dashes and four dots is drawn through points calculated from Eq. (22), using the effective mass of 0.43 m_e (velocity averaging over the Druyvesteyn distribution). The other two curves in the figure (the dotted curve and the mixed dash and dot curve) represent the mobility values calculated from Eqs. (19) and (22) ($m^*=m_e$) and arbitrarily scaled upward for the purpose of easier qualitative comparison with the solid experimental curve. (Before scaling the mobility values agree with experiment within a factor of 2.)

agrees quite nicely with the bubble model,[13,14,48] since work must be done against the contractile forces of the liquid to create the void in which the electron traps itself.

The electron trapped in the bubble is only of lower free energy than the free-electron state because of the large, short-range repulsive interaction potential between the electron and the helium atoms. The electron-atom interaction potentials for argon, krypton, and xenon are strong and attractive (negative scattering length) but of long-range. For this reason, cavity formation is not expected to be favorable, and the quasi-free electron state should be lower in energy. Neon should be a particularly interesting fluid to study, since its small positive scattering length[49] of $+0.24a_0$ (a_0 is the Bohr radius) indicates a short-range, weak repulsive interaction potential. The assumptions used in the development of the theory are most closely satisfied for weak, short-range interaction potentials.

[48] B. Burdick, Phys. Rev. Letters **14**, 11 (1965).
[49] T. F. O'Malley, Phys. Rev. **130**, 1020 (1963).

It is clear from Fig. 5 that none of the elementary theories quantitatively account for the temperature dependence of the electron mobility in liquid argon. For all the theoretical calculations plotted in this figure, we have used the effective mass of the electron (0.43 free-electron masses) obtained from the exciton spectra in solid argon.[50] The physical picture of a weakly coupled exciton (Wannier exciton) is that of an electron describing a large orbit about a hole and enclosing many atoms of the medium within the domain spanned by the orbit. The dielectric screening of the atoms of the medium dispersed between the electron and the hole significantly weakens their Coulombic interaction.

There is an analogy between this physical picture of the weakly coupled exciton and that of an electron with a large mean-free-path in the liquid state. In our presentation of the elementary theory, we have considered the electron-atom elastic-scattering cross section to be unmodified, in itself, in the dense medium. However, the dynamics are affected by the electronic structure of the surrounding medium, and we have supposed that this leads to the inertial response of the electron being the same in the solid and the liquid. Clearly, this is a crude approximation, but we can do no better at present.

The thermodynamic data required for all the calculations were obtained from polynomial fits to the PV data of Dr. Johanna Levelt-Sengers.[51]

In Fig. 5 we observe that the best quantitative agreement is achieved with that theory which averages the electron velocity over the equilibrium Maxwellian distribution. We shall label this as theory I [Eq. (19)]. The negative slope of the temperature dependence predicted by theory I is too large by a factor of 2. Theory II [Eq. (22)], i.e., that theory in which we average the velocity over the Druyvesteyn distribution, underestimates the mobility in magnitude by a factor of 1.5. It is interesting to note that if the dotted line representing Theory II in Fig. 5 is scaled upward by this factor of 1.5, the scaled curve has a slope very close to the linear fit to the experimental values. This would seem to indicate that the correct dependence of the electron mobility on ρ_N and κ_T is in the combination $(\rho_N\kappa_T^{1/2})^{-1}$. In contrast to theories I and II, which underestimate the magnitudes of the mobility, the more general theory III [see Eqs. (6), (7), (9), (10), and (14)] predicts electron mobilities which are about 50% too large. The slope predicted by theory III is only 50% of the negative slope of the experimental line.

If the data given in Fig. 9 are examined, it is readily seen that none of the theories consistently predict both the temperature and electric field dependence of the experimental data. In the range of temperatures for which isotherms have been plotted in Fig. 9, the experimental values fall on linear plots which naturally extrapolate to the origin. This shows that the electron mobility is field independent in this range of temperatures. This behavior is characteristic of theory I. It has also been shown that perhaps the most important feature of the data plotted in Fig. 5, viz., the negative slope of the temperature dependence, is best described by theory II. Unfortunately, this theory also predicts that the electron-drift velocity should depend on the electric field strength as $E^{1/2}$. Clearly, the experimental data presented in Fig. 9 are linear in the electric field strength, in complete disagreement with this prediction. The electric field dependence of the electron drift velocity predicted by theory III (the curved line in Fig. 9 and the calculated values in Table V) does not agree with the experimental results at all. In fact, this plot merely reflects the effect of the Ramsauer minimum in the *gaseous* momentum-transfer cross-section (unperturbed by interactions of the dense fluid) which has been used in our calculations of the electron drift velocities in the *liquid*. This curve is very similar in form to the electric field dependence of the electron drift velocity in gaseous argon.[3]

An important characteristic of the isotherms presented in Fig. 9 is their striking linearity in that range of temperatures in which the negative slope of the temperature dependence is crudely predicted by the elementary theories. At these temperatures we can appropriately discuss an electron mobility. It is also important to notice that the linear dependence of the electron drift velocity extrapolates quite naturally to the origin, as, indeed, it must ($v_d=\mu E$). The slopes of these straight lines represent genuine mobilities. However, in the temperature ranges within which liquid krypton and liquid argon anomalously show a rise in the apparent electron mobility with an increase in temperature, the electron drift velocity is definitely nonlinear with respect to the electric field strength. This is clearly shown in Fig. 10. Wannier[31] has shown that at high-field strengths there should be an $E^{1/2}$ dependence of the electron drift velocity. The experimental points do not fit [Eq. (2)] an $E^{1/2}$ dependence (the solid curves in Fig. 10) as well as the fit which includes some linear dependence on E (the dashed curves in Fig. 10). This suggests that the experiments were not performed at high enough electric field strengths to observe a pure $E^{1/2}$ dependence and instead are in an intermediate-field region. The reader should not attach too much significance to these arguments, since the number of data points on which they are based is so small (three points).

The most intriguing feature of the data for liquid argon is represented by the minimum in the extended temperature dependence displayed in Fig. 6. We have not been able to complete enough successful experimental runs to pinpoint the temperature at which the minimum occurs (because of the great difficulties encountered in the purification of the gas). Nevertheless, it is important to notice that in the temperature range from 85–111.5°K, where the electron mobility decreases

[50] G. Baldini, Phys. Rev. **128**, 1562 (1962).
[51] J. Levelt-Sengers, (private communication).

with an increase in temperature in qualitative agreement with the elementary theories, the electron mobility is independent of the electric field strength. Even though we only have data on the electric field dependence at one temperature (145°K) above 111.5°K, we suggest that there may be a direct correlation between the onset of the electric field dependence and the change of the sign of the slope of the mobility curve displayed in Fig. 6.

We also observe an anomalous temperature dependence for the electron mobility in liquid krypton, which is displayed in Fig. 11. The electron mobility *increases* over the entire range of temperatures from 120–180°K and is dependent on the electric field strength at two temperatures in this range (see Fig. 10). This is similar in behavior to the case of liquid argon, where the mobility appears to be field-*dependent* in the range of temperatures in which the apparent mobility increases with an increase in temperature (see Fig. 9). However, at 185°K the mobility appears to decrease; and if the end of this curve is extrapolated to the isolated point at 200.9°K, an apparent maximum develops in the temperature dependence. We do not believe that this decrease in mobility is a pressure effect, on the basis of the observed pressure independence of the apparent electron mobility data for liquid krypton over the range of pressures from 5–33 atm (see Fig. 12). Unfortunately, we have only been able to obtain this one isolated point at temperatures above 185°K. The purification procedure becomes exceedingly difficult when the activated-charcoal trap cannot be cooled to temperatures below the temperature of dry ice. In fact, we were only able to observe electron current for a period of 30 min in this particular run, taken with Freon-22 (b.p. = 232°K) as the refrigerant for both the charcoal trap and the cell.

The theoretical discussion shows that the scattering of the electron by the fluid is weak. Therefore, we cannot neglect the consideration of the influence of impurity scattering on our results. It can easily be shown that neutral impurities[52] would have to be present in amounts which are very improbable in order for the scattering by these species to be dominant. However, a simple calculation using the results of Conwell and Weisskopf[53,54] for impurity *ion* scattering in dilutely doped semiconductors shows that charged impurities could affect the measured drift velocities at concentrations of less than 1 ppm. Such a low impurity concentration cannot be ruled out offhand. The total observed current ($\sum_i n_i v_i$, where n_i is the number density of charged species i, and v_i is the drift velocity of charged species i) is overwhelmingly due to free electrons, even if an appreciable amount of the charges are ions, because the electron drift velocity is greater than the ion drift velocity by a factor of 10^5. Prior to the electrolytic purification and the observation of free-electron drift velocities, our measured currents (ion currents) were 10^{-13} to 10^{-12} A, and the maximum ion concentration is then 10^7 to 10^8 ions/cc. We should also point out that this concentration of ionic impurities should not change much with temperature, since the concentration of neutral electron-trapping impurities is greater than the maximum negative ion concentration by several orders of magnitude.

Simple arguments lead to the conclusion that ordinary impurity scattering cannot consistently explain the discrepancy between elementary theory for scattering by atoms of the fluid and experiment. If the scattering by charged impurities were dominant, one could have a linear relation between v_d and E. Scattering by charged impurities is proportional to $T^{-3/2}$. If at lower temperatures, where the linear relationship between v_d and E has been observed in contrast to the theoretical expectations of elementary theory, the mobility would be limited by impurity scattering, it should increase with temperature, whereas, in fact, it decreases. Furthermore, the absolute value of the measured mobility is not too different from the value calculated from elementary theory, which again rules out charged-impurity limited mobility (contributions to the observed mobility from various scattering mechanisms combine as the sum of the inverse mobility values calculated for each mechanism.).[16] Consequently, other contributions to the observed mobility must be of the same order of magnitude as that calculated by elementary theory for scattering by the fluid atoms, and none of these contributions can then be dominant.

If scattering by neutral impurities were the dominant mechanism of scattering, one could *not* expect a linear relation between v_d and E except at improbable concentrations. It is clear that if neutral impurity scattering is dominant and the scattering cross section for the impurity is not much perturbed by the surrounding dense medium of fluid atoms, one essentially has a problem of electron scattering from a "gas" of impurities immersed in a background continuum of dielectric constant ϵ ($\epsilon \approx 1.5$ for liquid argon and this is close to the vacuum value). The mean-free-path is approximately $N^{-1/3}$, where N is the number density of impurity atoms, and at STP one would expect the electron drift velocity to be nonlinear in the electric field strength at about 1 V/cm ($N \approx 10^{19}$ cc^{-1}). Moreover, the electron energy under the conditions described above is sufficiently low that the cross-section for inelastic scattering by molecular impurities is small. Molecular impurity cross sections do not vary much with electron energy (no Ramsauer effect),[55] and one would expect the mobility limited by this type of scattering to be rather insensitive to temperature variation, contrary to experimental observation. Generally, it

[52] C. Erginsoy, Phys. Rev. **79**, 1013 (1950).
[53] E. Conwell and V. F. Weisskopf, Phys. Rev. **77**, 388 (1950).
[54] C. Kittel, *Introduction to Solid State Physics* (John Wiley & Sons, Inc., New York, 1956), p. 361.
[55] N. F. Mott and H. S. W. Massey, *Theory of Atomic Collisions* (Oxford University Press, London, 1965), 3rd ed., p. 588.

seems impossible to explain the minimum of the mobility-versus-temperature curve, shown in Fig. 6, by any mechanism where impurity scattering is assumed to be of dominant importance.

In theory I we considered the elastic-scattering cross section to be independent of velocity (energy) by taking the $K=0$ limit for the electron energy. However, the anomalies we find in the temperature dependence of the apparent electron mobility in both liquid argon and krypton cannot be explained by the constant-cross-section theories I and II. Most likely, the explanation of these anomalies will be found in a sensitive energy-dependent cross section (different in the liquid and gas), coupled with subtle changes in the high-velocity region of the electron-energy distribution with temperature variation. The calculations of the momentum-transfer cross sections and the electron-energy distributions in rare gases by Frost and Phelps[3] show that this is a reasonable viewpoint.

An important feature of the Frost and Phelps data is the Ramsauer minimum at electron energies of about 0.3 eV. There is also a rapid variation of the cross section in the energy range from 0.05 to 1 eV.[56]

Equation (7) shows that f_1 depends on the rate of change of the leading term in the expansion of the electron energy distribution. In turn, the electron-drift velocity depends on f_1 [see Eq. (9)]. An examination of the electron-energy distribution functions for gaseous argon, given in Fig. 5 of the paper by Frost and Phelps,[37] shows that the major contribution to $f_1(\epsilon)$ comes from the rapidly descending high-energy side of the distribution function. Since f_1 determines the drift velocity, it is clear that the high-velocity tail of the distribution function is dominant in the determination of the electron-drift velocity. It is precisely this part of the distribution function which undergoes the greatest change upon variation of the temperature. Moreover, the small number of electrons in the high-energy tail of the distribution are in an energy range where the scattering cross section is varying most rapidly with energy. Thus, the sensitivity of the electron-drift velocity to temperature variation is further increased, since the cross section, in turn, determines the energy distribution function and its high-energy tail.

Direct calculation of the drift velocity shows, however, that the theories described thus far do not give rise to an anomalous temperature dependence (Fig. 6). In the calculations mentioned (a portion of which have been displayed in Tables IV and V), the K dependence of the interference function has been neglected, and we have used the *single* atom elastic scattering cross section from *gas* phase data without modification. These are, of course, rather severe approximations. Lekner[32] has calculated electron drift velocities via Eq. (9) using the full $a(K)$ to modify the gas phase cross section according to Eq. (14). He finds that this modification of the calculation introduces only a 20 % decrease in the values displayed in Tables IV and V and Figs. 5, 9, and 13.

Clearly, that part of the calculation which is most sensitive to error is the introduction of the energy-dependent cross section. We have already observed that the cross section not only enters the calculation of the drift velocity directly, but also indirectly in its determination of the energy distribution function itself. We conclude that a successful explanation of the complete experimental temperature dependencies requires accurate experimental data on the elastic scattering cross-section in the *liquid* phase or a more accurate theoretical calculation of the effective cross section in the liquid state.

Recently, Lekner[32] has shown that, assuming a pseudopotential for the electron-atom interaction consisting of a repulsive core and an attractive long-range tail (the parameters of this pseudopotential without screening were adjusted to fit the gas-phase cross-section data of Frost and Phelps[3]) with a variable amount of dielectric screening, the Ramsauer minimum in the cross section becomes deeper and shifts to lower electron energies with increased screening. This important result strongly supports, for the first time, the plausibility of a Ramsauer minimum in a scattering process in a condensed phase. Lekner is presently pursuing the problem in greater detail. A local-field function, $h(r)$, which modifies the Coulombic field (due to the electron alone) to account for dielectric screening, may be directly related to the pair correlation function, $g(r)$. Using the Percus-Yevick hard-sphere correlation function[45,46] for liquid argon at 84°K, Lekner has numerically evaluated $h(r)$. This function has a sharp minimum at approximately $r=\sigma$, where σ is the Lennard-Jones parameter, and this minimum corresponds to a maximum in the screening. This function, $h(r)$, is used in the calculation of the cross section; and it is very sensitive to temperature. This sensitivity may lead to an explanation of the anomalous temperature dependencies we observe.

All the calculations reported in this paper (see Tables IV and V) use the *total* elastic-scattering cross section. This is only valid if the differential elastic-scattering cross section, $\sigma_s(\theta,\phi,v)$, is independent of angle. Of course, since $\sigma_s(\theta,\phi,v)$, is generally unknown, even in the gas phase, we are forced to use the total cross section or nothing. The reader should note that $a(K)$ is a function of angle, and thus, if σ_s is a function of angle also, they are coupled in the integrand of the complete integral for the liquid-phase cross section

$$Q_L(v)=\int_0^{2\pi}\int_0^{\pi} a\left(2k\sin\frac{\theta}{2}\right) \times\sigma_s(\theta,\phi.v)(1-\cos\theta)\sin\theta d\theta d\phi\,. \quad (23)$$

[56] We are indebted to Dr. L. S. Frost and Dr. A. V. Phelps for presenting to us their cross section data as a function of energy in a convenient tabulated form.

The pressure dependence of the apparent electron mobility in liquid argon is displayed in Figs. 7, 8, and 13. At 145°K the apparent electron mobility decreases with pressure sharply. Elementary theories cannot yet explain this behavior.

At all other temperatures for which we have plotted pressure dependencies (except 90°K), the elementary theories predict the qualitative increase in the electron mobility with an increase in pressure fairly well, with theory II once again being the most successful when the values are increased by an appropriate scale factor. These comparisons between the predicted and the experimentally observed pressure dependencies are shown in Fig. 13.

There appears to be no significant pressure dependence of $\langle\tilde{\mu}\rangle$ in liquid krypton for the range of pressures and temperatures studied. This is clearly demonstrated in Fig. 12.

Let us now summarize the successes of the elementary theories. As a zero-order description, it is quite remarkable that the elementary theories are in agreement with the experimental observations to within a factor of 2. This must be considered as a major success and indicates that the most important physical processes are properly accounted for. Theories I, II, and III all predict a decrease in the electron mobility with an increase in temperature. This, of course, is in qualitative agreement with the results plotted in Fig. 5. It is also very interesting to notice the excellent qualitative agreement of both the temperature (Fig. 5) and pressure (Fig. 13) dependencies of the mobility values calculated from Eq. (22). The excellent agreement between experiment and theory, when it is *assumed* that the field energy of the electron is much greater than the thermal energy, tends to rule out any hypothesis that the electrons are in thermal equilibrium with the fluid. From these successes, we are led to believe that the fundamental approach involved in the zero-order approximation is correct.

However, we cannot ignore the failure of all the theories presented to explain the anomalous features present in the experimental results. From the large mean electron energies calculated for the low-electric-field strengths used in our experiments, it would appear that the electrons are *not* thermal for electric field strengths above 1 V/cm. If this is correct, it seems unlikely that any simple theory will predict the striking (observed) linearity in the field dependence of the electron drift velocity at the "high" electric field strengths used in our experiments (see Fig. 9). In fact, all the refined calculations using the procedure outlined in theory III show a behavior which is much closer to the results plotted in Fig. 10. The amazing linearity of the experimental data presented in Fig. 9 appears to be one of the most interesting and puzzling features of our data.

The anomalous rise of the apparent electron mobility in both argon (Fig. 6) and krypton (Fig. 11) strongly suggests that there is a Ramsauer minimum in the elastic-scattering cross section in the liquid state. This conjecture has not been supported by any of the calculations reported herein, all of which use the *gas* phase energy-dependent cross sections. However, in Fig. 3 of the paper by Frost and Phelps,[37] there is a maximum in the apparent electron mobility in *gaseous* argon in correspondence with the minimum in the cross section. A minimum in the elastic-scattering cross section for the liquid, which, most likely, is of a different form and at a different location on the energy scale, may explain the "maximum" in the experimental apparent electron mobility as a function of temperature. We must await either further experimental data on electron drift velocities and elastic-scattering cross sections for the liquefied rare gases, or detailed theoretical calculations of the liquid-phase elastic-scattering cross section which now are in progress[32] before we can completely understand the experimental data presented in this paper.

Finally, it is interesting to notice that the magnitude of the electron mobilities presented in this paper are comparable to electron mobilities in single crystals of semiconductors, such as diamond (1800 $cm^2\ V^{-1}\ sec^{-1}$) and germanium (3800 $cm^2\ V^{-1}\ sec^{-1}$).[57] Our mobilities also compare favorably with the preliminary measurements of A. H. Samuel *et al.* on electron mobility in high-purity liquid hexane (20 to 200 $cm^2\ V^{-1}\ sec^{-1}$).[58]

ACKNOWLEDGMENTS

We are indebted to John Lekner and Professor J. Jortner for helpful discussions.

We wish to thank the Directorate of Chemical Sciences, AFOSR, the USPHS, the NSF, and the Petroleum Research Fund of the ACS for financial support. We have also benefited from the use of funds provided by ARPA for materials research at the University of Chicago.

APPENDIX: OPERATION OF THE DRIFT-VELOCITY SPECTROMETER

An analysis of the operation of the gating system of electrical grids shown schematically in Fig. 2 has been given by Reif and Meyer.[16] In this Appendix we wish to explicitly derive second-order effects, which are merely stated in their analysis, and show that these second-order effects are indeed observed in our experimental results.

Suppose the pair of grids S and A (1 mm apart), forming the electrical shutter SA in Fig. 2, opens at times $k\Theta(k=0, 1, 2, \cdots)$ for a time $\tau=f\Theta$, where $f=\frac{1}{2}$ for the balanced square wave input to the electrical gates SA and BB′ and Θ is the period of this square wave. The electrons arrive in front of grid B in pulses of duration $\tau-T_1$ at times $k\Theta+T_1+T_0$, where T_1 is

[57] G. Kittel, Ref. 54, p. 352.
[58] A. H. Samuel, F. O. Halliday, A. K. Keast, and S. I. Taimuty, Science **144**, 839 (1965).

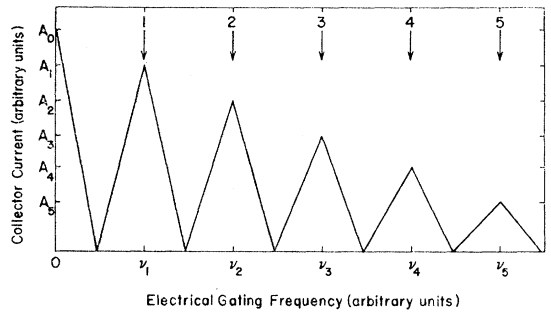

FIG. 14. The collector current plotted as a function of the electrical shutter frequency as it is calculated from Eq. (26). The relative amplitudes, A_m, and the asymmetry of the peaks, χ, are calculated using the experimental values of $g_s(0.085\bar{1})$ and $f(0.5)$. The corresponding experimental plot is displayed in Fig. 3.

the time required for the electrons to drift across the finite width of the electrical shutter space SA, and T_0 is the time required for the electrons to drift the distance AB between the shutters SA and BB′. Let us define a relation between three sets of integers m, n, and k to be $n-k=m$. We also define a time $\delta\Theta(-1<\delta<1)$ representing the difference between the time of opening of shutter BB′ and the arrival of the leading edge of an electron pulse at B. Let θ equal the fraction of the pulse which is transmitted by gate BB′$(0\leqslant\theta\leqslant\tau-T_1)$. Clearly, T_1+T_0 is a fixed quantity for constant temperature, pressure, and electric field strength, and it may always be related to Θ by the relation

$$(n+\delta)\Theta=k\Theta+T_1+T_0. \tag{24}$$

Using this fundamental relation, we consider three distinct cases:

(a) $\delta=0$. Physically, it is clear that this corresponds to the case when the entire electron pulse is transmitted past the gate BB′ (maximum current transmission). For this case one can readily rearrange Eq. (24) to give

$$\nu_m{}^{(0)}=m\nu_1{}^{(0)}=\frac{m}{T_1+T_0}=\frac{m}{T_0(g_t+1)}. \tag{25}$$

where $g_t=T_1/T_0$, $\nu_1{}^{(0)}$ is the fundamental frequency corresponding to the first maximum in the collector current versus gating-frequency profile (see Figs. 3 and 14), and $\nu_m{}^{(0)}$ is the mth harmonic corresponding to the mth maximum in the collector current ($\nu_m{}^{(0)}=\Theta_m{}^{-1}$, see Fig. 14).

We define a relative integrated electron current $A=\theta/\Theta$, relative to the current collected at C when the electrical shutters SA and BB′ are continuously in their open phase (solid line configuration in Fig. 2). The relative electron current at the mth maximum is then given by

$$A_m=\frac{\theta_m}{\Theta_m}=\frac{f\Theta_m-T_1}{\Theta_m}=f-\frac{g_t m}{g_t+1}, \tag{26}$$

where we have substituted from Eq. (25) and used the relation $\nu_m{}^{(0)}=\Theta_m{}^{-1}$.

(b) $\delta>0$, $\delta=\delta_+$. This condition on δ corresponds to the case of the gate BB′ opening *before* the electron pulse arrives at B. Then

$$A_m{}^+=\frac{\theta_m{}^+}{\Theta_m{}^+}=\frac{(\tau_+-T_1)-\delta_+\Theta_m{}^+}{\Theta_m{}^+}$$
$$=f+m-\frac{(2T_1+T_0)}{\Theta_m{}^+}, \tag{27}$$

where we have substituted for $\delta_+\Theta_m{}^+$ using Eq. (24).

(c) $\delta<0$, $-|\delta|=\delta_-$ This condition on δ corresponds to the case of the gate BB′ opening *after* the leading edge of the electron pulse has arrived at B. For these conditions we write

$$A_m{}^-=\frac{\theta_m{}^-}{\Theta_m{}^-}=\frac{(\tau_--T_1)-\delta_-\Theta_m{}^-}{\Theta_m{}^-}=f-m+\frac{T_0}{\Theta_m{}^-}, \tag{28}$$

where we have substituted for $\delta_-\Theta_m{}^-$ using Eq. (24).

The frequency $\nu_m{}^{(-)}=[\Theta_m{}^-]^{-1}$ at which $A_m{}^-$ falls to zero is $(m-f)/T_0$ [set Eq. (28) equal to zero]; the frequency $\nu_m{}^{(+)}=[\Theta_m{}^{(+)}]^{-1}$ at which $A_m{}^+$ falls to zero is $(f+m)\cdot[T_0(2g_t+1)]^{-1}$ [from Eq. (27)]. From these expressions and Eq. (25) we observe that there is an apparent asymmetry to the peaks in the collector current shown in Fig. 14, which is given by the relation

$$\chi=\frac{\nu_m{}^{(0)}-\nu_m{}^{(-)}}{\nu_m{}^{(+)}-\nu_m{}^{(0)}}=1+2g_t. \tag{29}$$

By this analysis we have shown that:

(1) For one charged species (one mean drift velocity) the collector current as a function of gating frequency will have distinct peaks at integer multiples of a fundamental frequency [Eq. (25)]. Several charged species of similar concentration and drift velocity would give a complex drift-velocity spectrum by the superposition of several elementary spectra. The simplicity of our experimentally observed spectra (see Fig. 3) confirms our belief that we are indeed observing one negatively charged species, the electron, and actually a *mean drift velocity* as opposed to a Maxwellian distribution of electron velocities;

(2) The successive harmonics or maxima in the current versus frequency (see Figs. 3 and 14) should decrease in intensity according to Eq. (26). It is important to notice that the correction factor required for all the equations describing the behavior of the nonideal gating system (nonideal because of the finite width of the electrical shutters SA and BB′) is g_t. Our experimental measurement of this correction factor does not give g_t but a quantity g_s, which is defined to be the ratio s_1/s_0, where s_1 is the distance between grids S and A (these two grids form the first electrical shutter) and s_0 is the distance between grids A and B. g_s and g_t are

related by the expression

$$g_s=\frac{\mu E_1 T_1}{\mu E_0 T_0}=g_t\cdot\frac{E_1}{E_0}, \tag{30}$$

where E_1 is the electric field across s_1 and E_0 is the electric field across s_0.

In our experiments f is equal to $\frac{1}{2}$ for the balanced square-wave input to the gating grids S and B′. Substituting g_s for g_t [by Eq. (30) this is only valid if $E_1=E_0$] in Eq. (26), the predicted ratio of the amplitudes of the successive harmonics ($g_s=0.0851$ in our experiments) is found to be $(A_2:A_3:A_4:A_5)_T=(3.2:2.5:1.7:1)_T$. In Fig. 3 a direct trace from one of our experimental recordings (for liquid Ar, $T=90.1°$K, $p=7$ atm, and $E=-200$ V/cm) is shown. The relative amplitudes of these experimental peaks stand in the ratio $(A_2:A_3:A_4:A_5)_{\text{exp}}=(2.6:2.1:1.6:1)$. Comparison of the ratio between a pair of successive peaks for *each* set of relative amplitudes shows that the experimental peaks decrease 3% less rapidly. This discrepancy is readily explained by the observation that we have used g_s in Eq. (26) and not g_t.

By Eq. (30) it is clear that this substitution is only valid if $E_1\equiv E_0$. However, the electric field, E_1, in the shutter space, s_1, is determined completely by the amplitude of the applied square wave, which is measured with an oscilloscope. The error in this measurement is of the order of 5%. The experimental ratios of the amplitudes may be reproduced from Eq. (26) if $g_t=0.0784$. The difference between this value for g_t and the measured value of $g_s(0.0851)$ is 9% and is of the same order as the error in E_1. Therefore, to this order of precision our experimental collector current–versus–frequency spectrum is consistent with Eq. (26) describing this second order effect.

At this point we should emphasize that a 10% error in the correction factor g_t only corresponds to a 1% error in $\nu_m^{(0)}$ (g_t is approximately 0.1) as given by Eq. (25), since in this g_t enters only in the factor $(1+g_t)^{-1}$. On the other hand, the relative amplitudes of the peaks [Eq. (26)] depend directly on g_t, and this second-order effect is much more sensitive to an error in g_t (by a factor of 10) than $\nu_m^{(0)}$.

The detailed analysis presented in the first paragraphs of this Appendix predicts an asymmetry in the peaks of the electron-current–versus–gating-frequency spectrum shown in Fig. 14. This asymmetry is described in terms of the asymmetry factor χ given by Eq. (29). From the third-harmonic peak in the experimental spectrum displayed in Fig. 3, we find a value of χ equal to 1.23. Replacing g_t by g_s (the experimentally determined g) in Eq. (29), we find $\chi=1.17$. This agreement is deceptively good, since $\nu_3^{(0)}$ is of the order of 200 kc/sec, and this frequency is not known to better than 1%. However, the differences $\nu_m{}^0-\nu_m{}^{(-)}$ and $\nu_m{}^+-\nu_m{}^{(0)}$ are of the order of 30 kc/sec and an error of ± 2 kc/sec in the numerator and denominator of χ can change χ by as much as 10%. It becomes clear that the asymmetry factor χ is so sensitive to the exact values of $\nu_m{}^{(+)}$, $\nu_m{}^{(-)}$, and $\nu_m{}^{(0)}$ that our experimental uncertainties are sufficiently large to preclude any possibility of a quantitative comparison between experiment $[\nu_m{}^{(0)}-\nu_m{}^{(-)}/\nu_m{}^{(+)}-\nu_m{}^{(0)}]$ and theory $(1+2g_t)$. We may only note that there is a definite asymmetry in the experimental peaks in qualitative agreement with Eq. (29).